Enhanced Photocatalytic Activity of Sol-Gel Derived Coral-like TiO_2 Nanostructured Thin Film

Bahramian, Ali Reza*[+]

Department of Chemical Engineering, Hamedan University of Technology, Hamedan, I.R. IRAN

ABSTRACT: *To enhance photocatalytic degradation of organic pollutants, coral-like TiO_2 nanostructured thin films were chemically synthesized through the sol-gel method. The fabricated thin films were characterized by Scanning Electron Microscopy (SEM), X-Ray Diffraction (XRD), nitrogen sorption isotherms, mercury porosimetry measurements, and UV-Vis Diffuse Reflectance Spectrum (DRS). The coral-like TiO_2 structures were assembled from cashew-like nanoparticles, which were composed of numerous highly crystallized in anatase phase. The assembled materials possess a high specific surface area of 167 m^2/g and mean pore size diameter of 12.3 nm. The coral-like TiO_2 nanostructured thin film shows a significantly higher photocatalytic activity than that of the commercial photocatalyst P25-TiO_2 based film on the degradation of Methylene Blue (MB) and Methyl Orange (MO). The high photocatalytic activity of film was ascribed to the large light absorption caused by small particle size, micro/meso and macropore structures, and pore scattering, reduced band gap energy, and reduced recombination of electron-hole pairs. These findings open up a new approach for promising environmental applications.*

KEYWORDS: *Thin film; Coral-like nanostructures; Sol-gel coating; Catalysis and surface analysis; Photocatalytic degradation.*

INTRODUCTION

It is comprehensively recognized that performance of nanomaterials is considerably interconnected to their controlled sizes, shape and morphologies. In recent years, fabrication of inorganic nanomaterials into 3D structures has attracted noteworthy research activities, caused by their potential applications in photocatalysis [1], membrane filters [2], gas sensors [3], dye-sensitized solar cells (DSSCs) [4], optoelectronic devices [5], and energy storages [4,6]. As a classical photocatalyst material, titanium dioxide (TiO_2) is extensively applied for decomposition of organic pollutants in air and/or water, because of its oxidizing authority, chemical stability, environmental compatibility, process ability, and low cost [1, 7-9]. The band gap energy of pure TiO_2 is larger than 3 eV (3.23 and 3.02 eV for anatase and rutile phase, respectively), thus making it especially active related to irradiation of UV ray [1, 5, 10]. When the electrons in anatase TiO_2 nanoparticles are irradiated by UV lights, they can be excited from the valence band to the conduction band to create electron–hole pairs [1, 10]. The holes produced in the valence band can react with organic molecules existing in water or air to obtain hydroxide radicals (·OH). Then, the photogenerated electrons are adequately diminished to generate superoxide (O_2^-).

* *To whom correspondence should be addressed.*
+ E-mail: bahramian@aut.ac.ir
1021-9986/2016/2/27-41 15/$/6.50

The redox potential of the electron–hole pair allows the formation of H_2O_2 molecules. Therefore, each of the produced species including ·OH radicals, O_2^{-}, and H_2O_2, based on the oxidation reactions, can act as oxidizing agents in order to enhance photocatalytic reactions rate. Recently, researches focused on the degradation of organic contaminants with enhanced photocatalytic activity using UV/H_2O_2/TiO_2 or Vis/H_2O_2/TiO_2 [10-12].

Outstanding to variable properties and wide applications, different shapes and morphologies of TiO_2 nanostructures have already been synthesized by several routes, including hydrothermal process, micro-emulsion, anodic oxidation, gas-phase oxidation, and sol-gel technique. Generally, TiO_2 nanostructures synthesized by the hydrothermal process lead to the formation of uniform structures [4, 13]. However, this technique is expensive and complex owing to the high rate of hydrolysis reaction of Ti-containing precursors in aqueous phase. Therefore, it is necessary to achieve easy and adequate methods for rational design of novel morphologies of TiO_2 nanostructures prepared with cost-effective approach.

Fabrication of nanostructured thin films has attracted attention caused by the substantial chemical and physical properties and potential applications in many technological fields. It was shown that two-dimensional (2D) TiO_2 nanosheets and three-dimensional (3D) flower-like TiO_2 nanostructures have superior photoelectron-catalytic and photovoltaic activities and solely novel reaction routes when their photocatalytic performance is compared to the microstructures titania [14,15]. *Zheng et al.* synthesized the hierarchical TiO_2 microspheres assembled from nanotubes, which exhibit good degradation ability to methyl orange associated with high specific area of 300 m^2/g [16]. They found that the specific surface area of the prepared film can play an effective role in the adsorption of molecules and charge transfer among the molecules. However, two other research groups showed that the flower-like hierarchical TiO_2 nanostructures show suitable photocatalytic activities at fairly low specific surface area (~70 m^2/g) [1, 17, 18]. Specific surface area of fabricated film may also affect electronic properties, interaction of molecules with surface defects and surface potential differences such as work function differences measured in aqueous solution. Despite the above-mentioned successful explanations, searching for novel procedures for rational design of the TiO_2 nanostructures is essential to get a high external surface area and superior photovoltaic properties.

In this study, sol-gel derived TiO_2 coral-like structures was chemically synthesized and physically coated on a soda lime glass using dip-coating process. The surface morphology of the prepared TiO_2 nanostructured films was comprised of macropores structures with a large fraction of micro and mesopores. The surface of prepared film shows much higher photocatalytic activities for degradation of Methyl Oange (MO) and Methylene Blue (MB), as common organic dyes, under UV irradiation than commercial P25 titania. The reasons for the enhanced performance and the factors affecting the photocatalytic activity of coral-like TiO_2 nanostructured films were analyzed by Scanning Electron Microscopy (SEM), X-Ray Diffraction (XRD), Brunauer-Emmett-Teller (BET) analysis and UV-vis spectroscopy. The procedure recommended in this work allocates explanation of the specific morphology of nanostructured film with high surface area and enhanced photocatalytic activity that can be applied in commercial scale for fabrication of high performance thin films.

EXPERIMENTAL SECTION

Chemicals.

Titanium tetra-isopropoxide (TTIP 99.9 %), hydrofluoric acid (37.43%, ACS reagent grade, EMD Chemicals), and ethanol (99.9%) were used as received. All chemicals used in this work were obtained from Sigma-Aldrich Co. Dionized water with a resistivity of 16.2 MΩ.cm was obtained from a deionized (DI) water filtration system.

Synthesis of TiO_2 nanoparticles.

At first, TTIP as a chemical precursor was gradually mixed with pure ethanol under vigorous stirring at room temperature. Second, a series of HF acids with different molar ratio are dissolved in deionized water under stirring at same condition. The molar ratios of the reactants were set as follows: TTIP: HF: C_2H_5OH:H_2O = 1:0.5:18:340 (symbolized as R1); TTIP: HF: C_2H_5OH:H_2O = 1:1:18:340 (symbolized as R2); TTIP: HF: C_2H_5OH:H_2O = 1:1.5:18:340 (symbolized as R3); TTIP: HF: C_2H_5OH:H_2O = 1: 2:18:340 (symbolized as R4), and TTIP: HF: C_2H_5OH:H_2O = 1:2.5:18:340 (symbolized as R5).

Finally, the TTIP-C_2H_5OH solution was gradually mixed into last one under stirring at the temperature of 90 °C. The obtained solution was allowed to react under stirring and refluxing to obtain a homogenous solution with milky color. Then, 60 ml deionized water was added to the obtained solution and allowed to stir slowly during 36 h at 50 °C to make sure that hydrolysis reaction was achieved and a solution with light bluish color appeared. More details on the procedure of TiO_2 synthesis are available in previous article [19].

Fabrication of TiO_2 films.

At first, a series of 10 × 10 mm square soda lime glasses as substrate were cleaned in an ultrasonic bath involving pure ethanol for 10 min. Then, the TiO_2 thin films were obtained by dipping substrates into TiO_2 solutions (corresponding to samples R1 to R5) by a high resolution dip-coater. A minimum withdrawal velocity, corresponding to 0.4 cm/min was applied during dip-coating process of each sample to obtain a homogeneous thin film. The fabricated films were preheated at 120 °C for 20 min and cooled down to ambient temperature. The similar procedure was repeated three times. Finally, the fabricated film was annealed at 350 °C for 1 h in vacuum condition with heat regime of 2 °C/min.

Film characterization.

The mean thicknesses of fabricated TiO_2 thin films were measured by a ZeScope optical profilometer. The surface morphology of the coral-like TiO_2 nanostructures was examined using a scanning electron microscopy (SEM, Cam Scan MV2300 microscope). The crystallite size and phase structure of TiO_2 was determined by X-Ray Diffraction (XRD) method based on the Debye-Scherrer formula using a Philips PW 1800 diffractometer with Cu Kα radiation. The specific surface area of the prepared films was determined by Brunauer-Emmett-Teller (BET) method using a surface area analyzer (Micromeritics ASAP 2020). Micro and mesopore size distribution was achieved by the Barrett-Joyner-Halenda (BJH) method based on the adsorption branch of N_2-sorption isotherms. The size of macropore volume of the TiO_2 structures was determined by mercury porosimetry measurements. UV-Vis diffuse reflectance spectra (DRS) of TiO_2 thin films were measured at room temperature using a spectrophotometer (Hitachi 3140) operating in the 300–1000 nm region.

Photocatalytic activity experiments and analysis.

The photocatalytic activity of TiO_2 nanostructured thin films has been determined by measuring the photocatalytic degradation of MB and MO, as common organic compounds, under UV light irradiation. To reach this purpose, the 10 × 10 mm square TiO_2 films were suspended within a closed glass cuvette filled with MB and MO solutions. The initial concentration, C_0, of MB and MO solutions was adjusted to 1×10^{-5} and 5×10^{-5} M, respectively. The glass cuvette has a transmission cut-off at wavelength of 352 nm. Thus, the near UV spectrum of 500 W UV-lamp as the light source was only permitted to reach the film surface. During 4 h, at different time intervals, the TiO_2 films were taken out of the cuvette glass and the transmittance spectrum of MB and MO solutions were measured using UV-Vis spectrophotometer. Before the irradiation of light, the aqueous solutions were continuously stirred for 2 h to attain the adsorption balance. All of the photocatalytic measurements were performed under UV light in ambient conditions. In order to compare the results obtained by fabricated TiO_2 films with already-existed ones, a commercial TiO_2 P25-based thin film (consisting crystal phases of anatase 90% + rutile 10% wt.) was purchased by Degussa GmbH, Germany. The fabricated TiO_2 P25-based film was applied for investigation into photocatalytic degradation of MB and MO solutions, based on the similar procedure mentioned above for prepared TiO_2 film.

RESULTS AND DISCUSSION

Morphology characterization.

Fig. 1 (a-e) shows typical low-magnification SEM images of the TiO_2 nanostructured thin films. Indexes a, b, c, d and e represent the SEM images of TiO_2 films derived from samples corresponding to R1, R2, R3, R4, and R5, respectively. It should be noted that the TiO_2 films obtained from samples R1, R2 … and R5 will be presented briefly as R1-, R2- … and R5-TiO_2 films in the following sections. Superficially, all images show that considerable quantities of coral-like TiO_2 structures agglomerate to form nonordered mesoporous on the surface of the film. However, the surface morphology of R2-TiO_2 and R3-TiO_2 thin films (Figs. 1b and 1c) show the structure is more homogenous than that of the films obtained by other samples (Figs. 1a and 1d). Often,

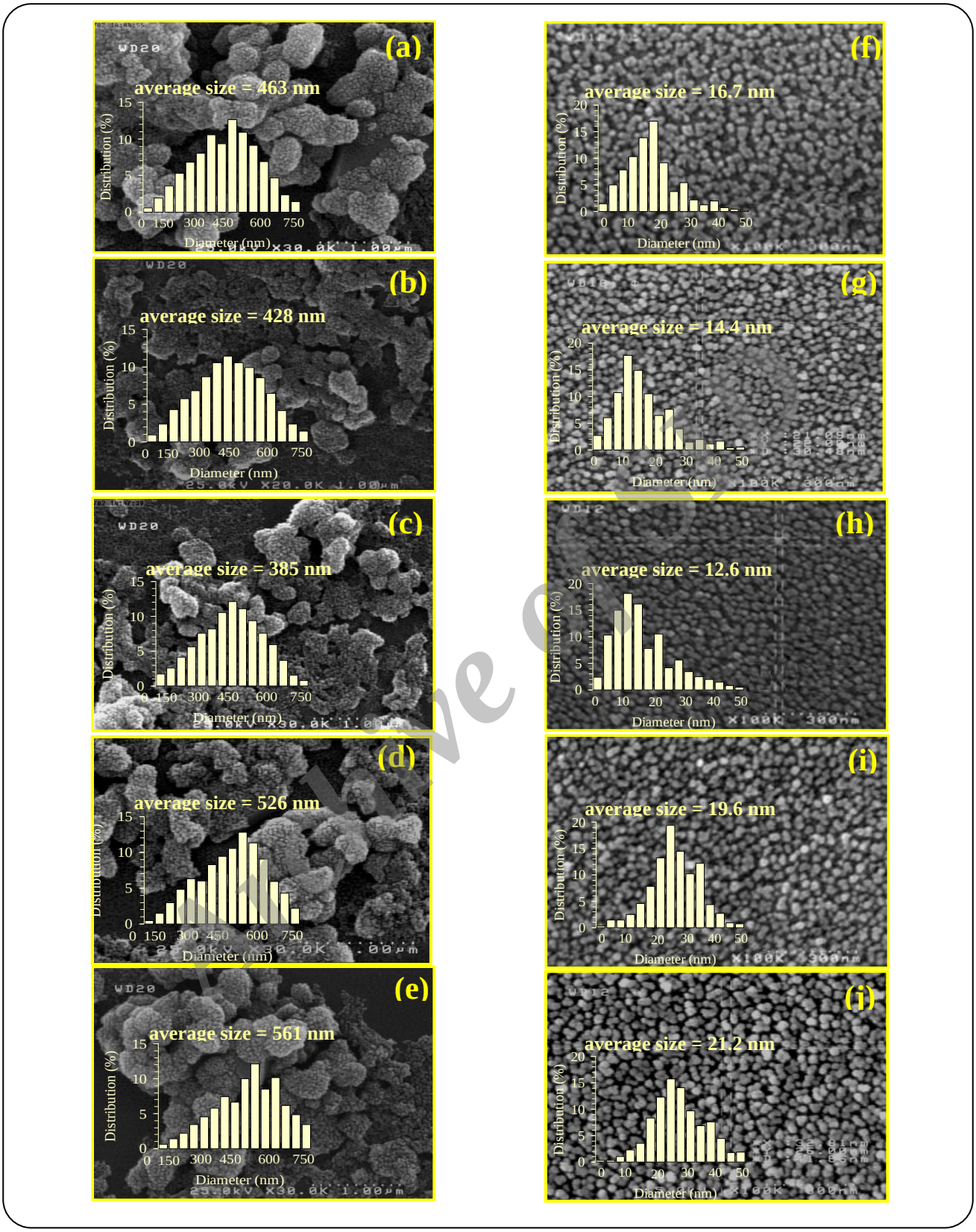

Fig. 1: SEM images of the TiO_2 nanostructured thin film fabricated from different samples (a-e) Low-magnification images, (f-j) High- magnification images: (a,f) R1, (b,g) R2, (c,h) R3, (d,i) R4 and (e,j) R5. All samples annealed at 350 °C.

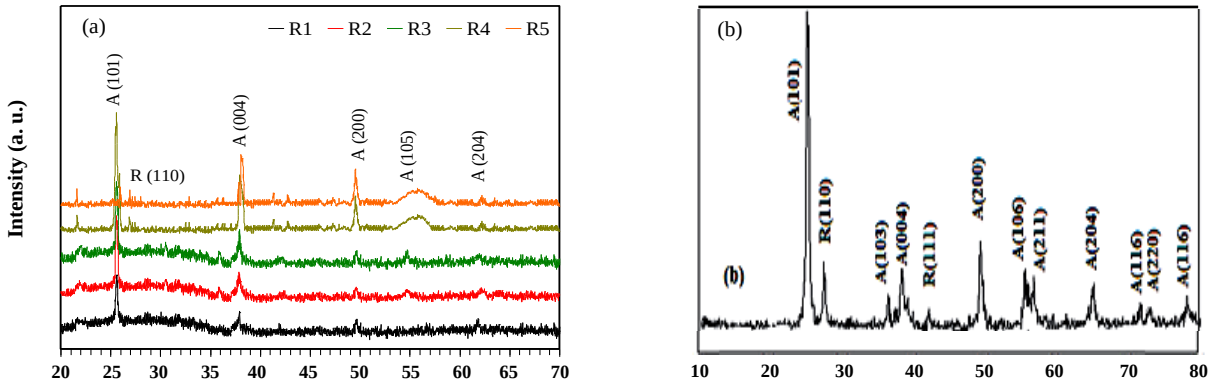

Fig. 2: XRD patterns for the (a) coral-like TiO_2 nanostructured thin films annealed at temperature of 350 ºC that obtained from samples corresponding to R1 to R5 and (b) P25-TiO_2 [27]. [A and R represents the anatase and rutile phase, respectively].

exact determination of the size of coral-shape structures is complicated owing to aggregated form of these structures. Nevertheless, it can be found that the size of mentioned structures is limited in the range of 100-750 nm. In addition, the coral-like TiO_2 structures seem to be formed by super-positing several layers, while the size of these structures differs spatially from lower part to the upper one. Based on the SEM image analysis, as shown in Fig. 1 (inset), the average size of the coral-like aggregates decreases from 463 to 385 nm for the R1-TiO_2 to R3-TiO_2 films, and then increases from 385 to 561 nm for the samples R3 to R5, respectively. The average size of the cashew-like particles formed on the aggregates decreases from 16.7 to 12.6 nm for the R1 to R3-TiO_2 films, and then increases from 12.6 to 21.2 nm for the samples R3 to R5, respectively.

Two common mechanisms of crystal growth mechanism may be used to describe the formation of the coral-like TiO_2 nanostructures. First mechanism is based on the aggregation of primary TiO_2 particles to form spherical small particles, which are relatively larger in size in compared with the primary species. The surface of the spherical small particles acts as nucleation sites to formation of small TiO_2 blisters. Regarding the energy level, formed blisters tend to grow and react with each other through shrinkages in coral-like structures. Another possible mechanism, which is named Ostwald ripening process, is based on dissolution of nanoparticles, followed by the growth of larger particles in the fast nucleation stage [20,21]. Based on this process, at first, nanoparticles with cashew-like forms are created on the surface of the coral-like structures during coarsening period. Then, using the Ostwald ripening process, the coral-like TiO_2 structures are formed on the film surface.

Further morphology characterization of the sol-gel derived TiO_2 nanostructured thin films (R1 to R5) is presented by the high-magnification SEM images in Figs. 1f to 1j, respectively. After magnification, it can be seen that the surface morphology of the coral-like structures is comprised of cashew-shape nanoparticles. Based on the N_2-sorption isotherms, it can be found that the size distribution of cashew-shape particles formed on the surface of films obtained from samples of R1, R2, R3, R4 and R5 were in the range of 25.78-35.22 nm, 23.44-38.07 nm, 12.89-17.61 nm, 21.09-30.48 nm and 32.81-41.86 nm, respectively. Therefore, it can be expected that the number of cashew-like particles per area unit of a coral-like structure formed on the surface of the R3-TiO_2 film (Fig. 1h) is higher than that of the other.

X-ray diffraction.

Fig. 2 displays the XRD patterns of the coral-like TiO_2 nanostructured thin film obtained from samples corresponding to R1 to R5 at annealing temperature of 350ºC. Therefore, the effect of annealing temperature on the phase crystallinity of TiO_2 nanostructured films was investigated in the previous study.[19] It showed that the heat treatment process plays a key role in the formation of crystalline phases. In the coral-like TiO_2 nanostructured film annealed at 350 °C, the dominant crystalline phase is anatase; while the weak rutile phase diffraction (110)

Table 1: The weight fraction of anatase and rutile phase of different prepared samples determined using XRD patterns.

Crystalline phase	Weight fraction (%) of samples				
	R1	R2	R3	R4	R5
Anatase	92	95	98	86	83
Rutile	8	5	2	14	17

Table 2: The typical average crystalline size of TiO2 nanostructured thin film annealed at temperature of 350 °C calculated from FWHM for different molar ratio of HF solutions.

Plane	Average crystalline size (nm)					
	R1	R2	R3	R4	R5	P25
(101)	13.4	13.1	12.3	14.4	15.7	15.2
(004)	21.5	20.0	19.2	21.7	23.4	24.0
(200)	15.2	14.6	14.1	17.1	18.8	18.5

was detected for the film annealed at 400 °C. With this description, the effect of the molar ratios of the HF applied during synthesis is only studied in this work. HF act as a capping agent by reversing the relative stability of (101) plane and promoting the growth of the plane of (001), which represent anatase TiO_2 phase [22]. As suggested in Fig. 2, TiO_2 diffraction peaks at 25.4º, 37.8º, 48.2º, 54.4º and 62.5º appeared that are referred to as the planes of (101), (004), (200), (105) and (204), respectively. The strong diffraction peak according to (101) plane, represent anatase crystal phase, while weak peak, according to (110) plane, suggest at 26.8º, denote rutile phase. Therefore, it can be found that anatase phase of TiO_2 was the dominant phase in all of the fabricated films.

The weight fraction of anatase and rutile phase is calculated from the XRD patterns, using the following equations: [23]

$$\text{Anatase (\%)} = [0.79\, I_A / (I_R + 0.79 I_A)] \times 100 \quad (1)$$

$$\text{Rutile (\%)} = \{1/[(I_R + 0.79 I_A)/I_R]\} \times 100 \quad (2)$$

where I_A and I_R are the peak intensities of (101) and the (110) planes reflections for the anatase and rutile phase, respectively.

As seen in the XRD patterns presented in Fig. 2, the phase evolution process of obtained TiO_2 nanostructured film depends on the molar ratio of HF molar ratio. Table 1 shows the weight fraction of anatase phase in the mixture of anatase and rutile determined from the XRD patterns and calculated based on Eq. 1. It can be found that a maximum weight fraction of rutile phase can be obtained from sample R5. As the HF molar ratio is raised to 1 (sample R2), and 1.5 (sample R3), the anatase is dominant phase. For example, it can be seen that the 98% weight fraction of anatase phase is obtained from sample R3. When the molar ratio of HF solution increased to 2 (sample R4) and then 2.5 (sample R5), a mixture of anatase (86 and 83 wt. %) and rutile (14 and 17 wt. %) is obtained, respectively.

XRD analysis suggested that the average crystalline size of TiO_2 nanostructured film depends on the molar ratio of HF solution (corresponding samples R1 to R5). Table 2 show the typical average crystalline size of TiO_2 nanostructured thin film calculated from full width at half-maximum of peak (FWHM). The average crystallite size varied between 13.4-21.5 nm and 13.1-20.0 nm in the R1 and R2-TiO_2 film, respectively. This value decreased slightly between the ranges of 12.3 to 19.2 nm in the case of film obtained from sample R3. Finally, the average crystallite size reached the maximum range value of 14.4-21.7 and 15.7-23.4 nm in the case of R4 and R5-TiO_2 films, respectively. The peak height shown in Fig. 2 corresponds to the increase in crystallite size of (004) plane in comparison with other planes. This result is in accord with the trend from SEM image analysis as shown in Fig. 1, where R3-TiO_2 nanostructured film shows lower average particle size distribution on the surface compared with other samples. Moreover, with respect to Tables 1 and 2, it can be found that the average crystallite size of sample R3, with maximum anatase phase (98 wt. %), has the smallest value compared to other samples.

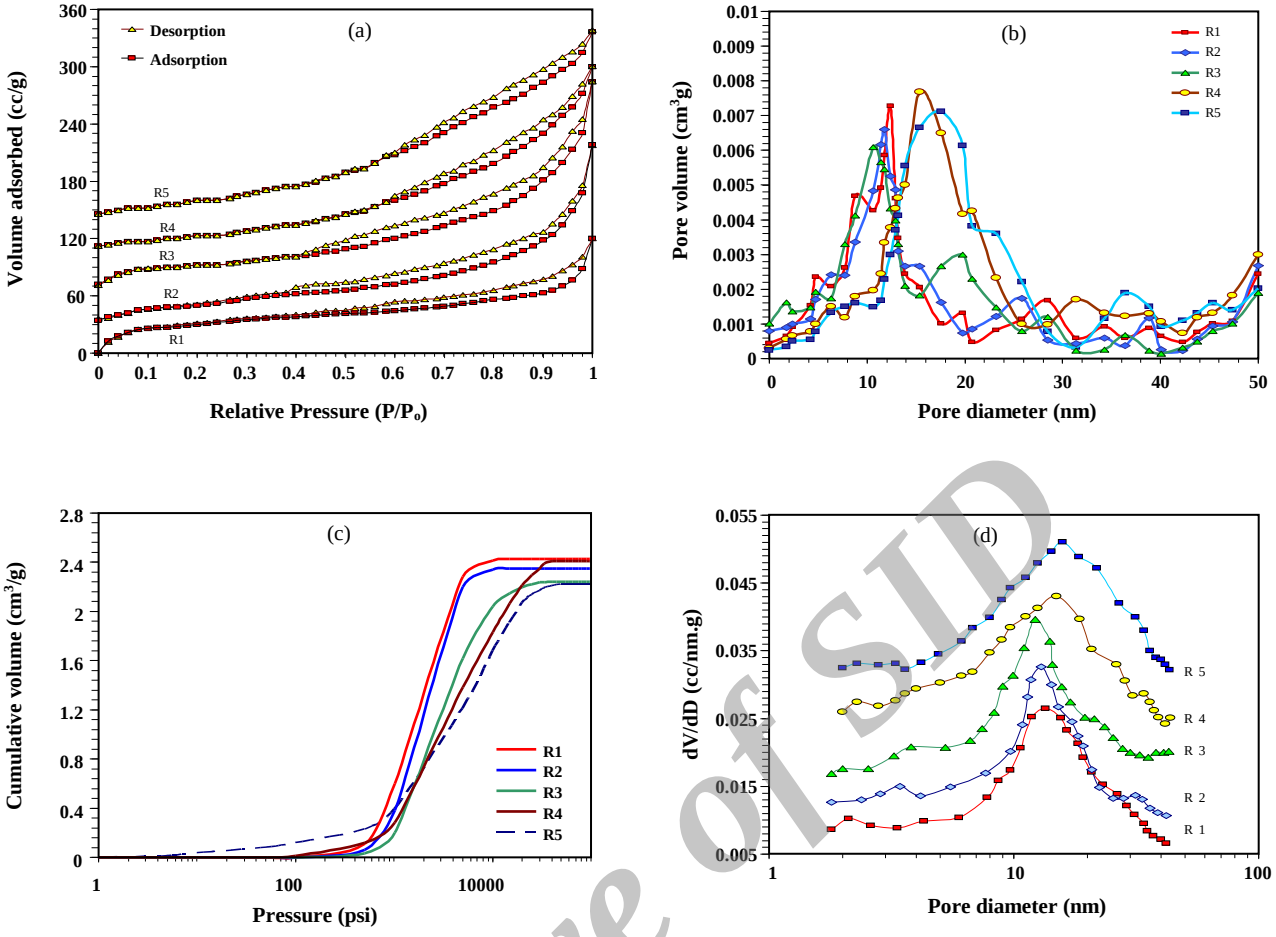

Fig. 3: Porous properties of the coral-like TiO_2 nanostructured thin films obtained from R1-5 samples. (a) N_2 adsorption-desorption isotherms, (b) micro and mesopore size distribution plots, (c) cumulative volume plots, and (d) macropore size distribution plots.

Surface area determination.

Fig. 3 (a-d) shows the porous properties of the coral-like TiO_2 nanostructured thin films annealed at 350 °C, obtained from samples corresponding to R1 to R5. N_2 adsorption-desorption isotherms are shown in Fig. 3a. According to this figure, two distinct capillary condensation curves of adsorption and desorption isotherms are observed. The first hysteresis curve is in the approximate range of $0.39 < P/P_o < 0.52$, in consistence with the filling of TiO_2 mesopore structures (pore size between 2 and 50 nm [25]) surrounded by intra-agglomerated primary nanoparticles. The second hysteresis curve is in the approximate range of $0.90 < P/P_o < 1$, in consistence with the filling of TiO_2 macropore structures (pore size greater than 50 nm [25]) assembled by inter-aggregated secondary particles, which are typical characteristics of macroporous materials. The hysteresis loop at $0.62 < P/P_o < 1$ in the case of sample R5 represents the hierarchical coral-like TiO_2 nanostructures, which can be seen from Fig. 1e. The BET specific surface areas, and pore diameters of R1 to R5-TiO_2 films are summarized in Table 1. BET surface area of coral-like R3-TiO_2 nanostructured film was estimated to be 167 m^2/g from adsorption curve in the range of P/P_0= 0.12-0.38, while average pore diameter of TiO_2 particles was determined to be 11.6 nm. The values of BET surface area and average pore diameter obtained from adsorption branch in the curve of R3, in the range of P/P_0 = 0.08-0.12 were estimated to be 162 m^2/g and 12.2 nm, while these values in the range of P/P_0=0.02-0.08 were estimated to be 155 m^2/g and 13.3 nm, respectively. These results of Table 1 showed that the BET surface area of coral-like R3-TiO_2 nanostructured film represents a maximum specific surface area of 167 m^2/g, which was higher than that

Table 3: Specific surface area, mean pore diameter and micro/meso/macropore volume of coral-like TiO_2 nanostructured thin films obtained from different samples.

sample	A_{BET} (m^2/g)	Mean pore diameter (nm)	Micropore volume (cm^3/g)	Mesopore volume (cm^3/g)	Macropore volume (cm^3/g)
R1	110	13.6	0.037	0.073	3.11
R2	159	12.8	0.034	0.069	3.02
R3	167	12.3	0.029	0.062	2.84
R4	107	14.9	0.041	0.077	3.25
R5	95	15.6	0.051	0.082	3.36
P25	63.0	21.1	0.060	0.085	3.80

of TiO_2 nanoparticles such as Aeroxide P25 reported in the literature (BET 50 m^2/g, 21 nm in diameter, anatase 80% + rutile 20%, Degussa) [7] and Aeroxide P90 (BET ≈ 90-100 m^2/g, 14 nm in diameter, anatase 90%+ rutile 10%, Degussa) [24].

The pore size distributions obtained using a DFT model is shown in Fig. 3b. The pore parameters are listed in Table 1. Fig. 3b shows that there is a small amount of mesopores. The volume of mesopores larger than 30 nm first increases then levels off with the increase of ratio of HF acid. However, there is no regular trend found for micropore sizes, but the volume of mesopores between 9 to 14 nm is the largest for the R3-TiO_2 film and the volume of mesopores between 25 to 34 nm is the largest for the R5-TiO_2 film.

Cumulative volume of the as-prepared films obtained from the samples R 1-5 is given in Fig. 3c. N_2 adsorption isotherms of the R1 to R4-TiO_2 films belong to type H1 adsorption hysteresis with reference to the IUPAC classification, which is characterized by porous materials [25]. These isotherms reveal a steep uptake at high relative pressures with no sign of leveling off due to capillary condensation mainly in the macropores. There is a small steep uptake of N_2 at low relative pressures at the initial part of these isotherms, which is characterized by micropore filling of N_2 with pore size smaller than 2 nm [25]. A small compression in the R5-TiO_2 film, as shown in Fig. 3c, exhibits H2 hysteresis according to the IUPAC classification that reveals a more complex pore structure of R5-TiO_2 film compared with other film samples because of the network effects (e.g., pore blocking/percolation) [25].

As the size of macropore volume of TiO_2 structures was out of the detection limit for N_2 adsorption measurement, experiments were carried out by mercury porosimetry method. Based on this, the macrpore size distribution of the as-prepared films obtained from the samples R 1-5 is given in Fig. 3d. The mercury uptake abruptly increases in pressures from 50 to 900 psi with the increase of the ratio of HF acid.

The micro/mesopore structures were primarily obtained from a difference of aggregated voids among the TiO_2 nanoparticles. The calculated pore sizes for the TiO_2 thin films obtained from samples R 1-5 are also given in Table 3. It can be found that the change in the molar ratio of HF applied during synthesis affects the pore size due to the crystal growth and shrinkage of the TiO_2 aggregates, resulting in a right and left shift of intra-aggregated and inter-aggregated pores, respectively [19]. The pore size distribution showed that the R2 and R3-TiO_2 films contained a smaller mean pore diameter (12.8 nm and 12.3 nm for samples R2 and R3, respectively) and exhibits a low micropore volume than that of the R1, R4, and R5-TiO_2 films. From Table 3, it can be found that the micropore volume of reveals a minimum and maximum value of 0.029 and 0.051 cm^3/g for the R3- and R5-TiO_2 film, respectively. In addition, the volume of macropores is considerably larger than the volume of micropore or mesopores. Therefore, the coral-like TiO_2 structures formed on the film surface have considerable amount of micro and mesopores with low amounts of macropores.

Photocatalytic reactions.

The photocatalytic activities of the coral-like TiO_2 nanostructured thin films obtained from different HF molar ratios, as a specific morphology-controlling agent, during synthesis reactions were evaluated by degradation of two common organic dyes, namely MB and MO, in aqueous solution under UV light irradiation. The results

corresponding to each analysis are presented in the following subsections.

Photocatalytic degradation of MB.

Fig. 4a shows typical UV-Vis adsorption spectra of MB in two forms of dispersed in dionized water and adsorbed on the coral-like R3-TiO_2 nanostructured thin film. The initial concentration of MB aqueous solution was adjusted to 1×10^{-5} M. Previous studies revealed that the absorption spectra of MB in water show a maximum absorption at about 660 nm, 610 nm, and 580 nm, for monomer, dimers, and aggregates form of MB dye, respectively [10]. Similar to previous studies, the MB aqueous solution indicates an absorption peak at ~660 nm, selected as reference value to study MB photocatalytic degradation in the presence of coral-like TiO_2 film. In the initial time of reaction (t = 0 min) absorption peak shows a maximum value at 610 nm, which presents the existence of dimers, while the adsorption curve shows a hypsochromic shift, *i. e.* 592, 588, 586, 581 and 578 nm, when UV irradiation time changed to 10, 30, 60, 120 and 240 min, respectively. In addition, the intensity of absorption peak significantly decreases with the UV irradiation time.

Generally, the photocatalytic degradation follows a Langmuir-Hinshelwood model [26]. The reaction rate equation for dye degradation can be written as follows:

$$r = -\frac{dC}{dt} = \frac{k_1 KC}{1 + KC} \quad (3)$$

Where C is the reactant concentration, t is the reaction time, K is the adsorption equilibrium coefficient and k_1 is the first-order rate constant in term of min^{-1}. If C is limited to very small value, Eq. 3 can be converted in the following integral form:

$$\ln\frac{C}{C_0} = k_{app} t \quad (4)$$

Where C/C_0 is the normalized dye concentration, and k_{app} is the apparent reaction rate constant.

Fig. 4b shows the photocatalytic degradation of MB solution versus time in the presence of coral-like TiO_2 thin films obtained from samples of R 1-5 (corresponding to curves a-e). For comparison, photocatalytic degradation curve of MB by P25 is also investigated under the same conditions (curve f). Clearly, after TiO_2 films are inserted into MB aqueous solution, the degradation efficiency of organic dye is changed considerably. After 240 min, it can be found that the degradation efficiency of studied MB solutions were 78.8% for sample R1 (curve a), 86.3% for sample R2 (curve b), 93.4% for sample R3 (curve c), 72.0% for sample R4 (curve d), 59.5% for sample R5 (curve e) and 68.5% for P25 (curve f).

Fig. 4c shows ln (C/C_0) versus irradiation time of coral-like TiO_2 thin films obtained from samples of R 1-5 (corresponding to curves a-e) and P25 (curve f). As shown, the adsorption of MB on the TiO_2 surface is quick while the highest and lowest equilibrium adsorption capacities are obtained from the samples of R3 and R5, respectively. It can be explained by this fact that the adsorption capacity increases with the increase of mean pore size and specific surface area of TiO_2 film. Therefore, exceptional high MB adsorption capacity of the R3-TiO_2 film can be attributed to its high fraction of small mesopores with mean size of 12.3 nm as revealed by size distribution of 9.7-19.5 nm (see Table 3), which lead to the higher percentage of TiO_2 exposed related to irradiated UV light.

As shown in Fig. 4c, the kinetic plots of all TiO_2 thin films are expressed through the linear regression analysis. The linear relationship of ln (C/C_0) with irradiation time less than 120 min reveals that the photocatalytic degradation of MB follows pseudo-first-order kinetics, while above 120 min; a deviation (indicated by dashed lines) from pseudo-first order kinetics model is observed for all samples. The highest deviations are observed for the R2-TiO_2 (16.9 %) and R3-TiO_2 (18.8%) films.

According to Fig. 4 (a-c), the following points should be noted: (1) The adsorption peak significantly decreases with the UV irradiation time. (2) The degradation of monomer form of MB showed a faster kinetic reaction in comparison with the dimer and aggregate forms. During chemical reaction, monomer form of MB was slightly converted to the dimer and then to the aggregate forms. This reaction exhibits a blue shift in absorption peak from ~660 to 610, and then to 581 nm, respectively. This peak shift, which is named hypsochromic shift, may be because of the formation of de-methylated dyes. (3) After 10 min irradiation, a new peak at 592 nm can be seen, corresponding to higher conversion order of monomer and dimers to aggregates form of MB in the solution.

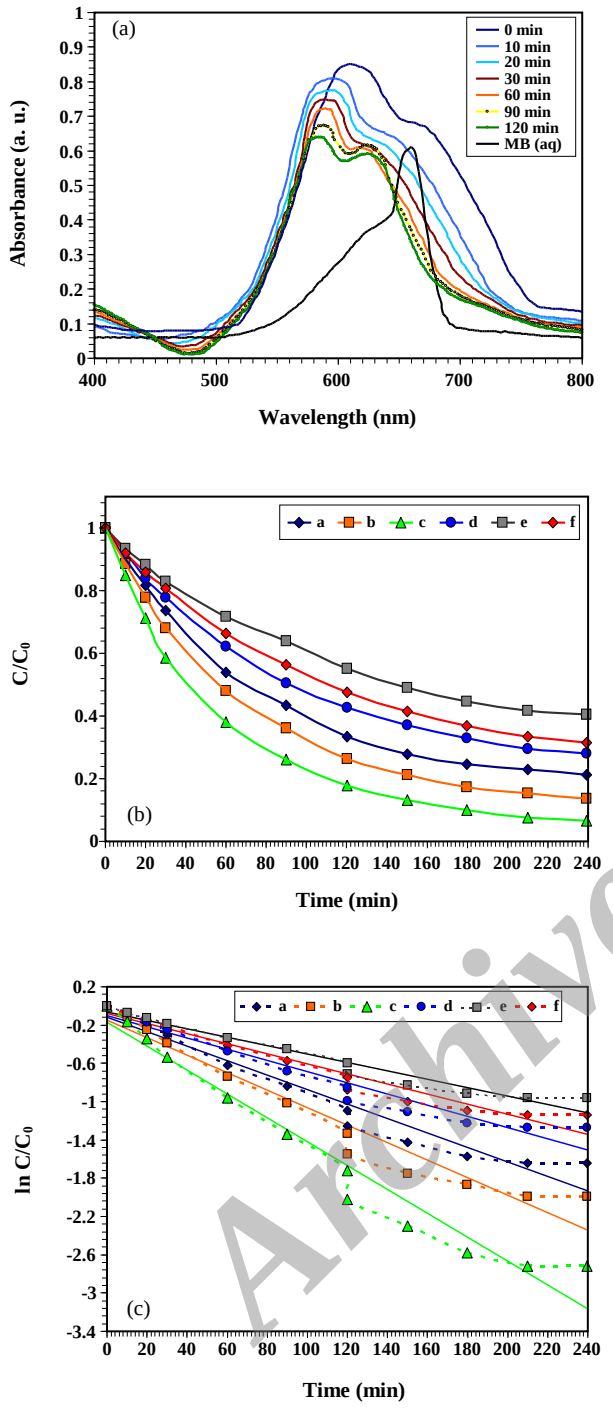

Fig. 4: Photocatalytic activities of coral-like TiO_2 nanostructured thin films in degradation of MB dye (1×10^{-5} M). (a) UV-Vis adsorption spectra of MB as a function of wavelength (dispersed in water and adsorbed on the R3-TiO_2 film) with different irradiation times. (b) Photocatalytic degradation of MB under UV light irradiation. (c) Pseudo-first-order kinetic rate plots for the datphotocatalytic degraion of MB. [a) R1, b) R2, c) R3, d) R4, e) R5, and f) P25-TiO_2 based film].

It suggests the fast monomer and dimmers related to degradation process in the first 10 min of reaction. Therefore, based on this adsorption process, it can be found that the formation of aggregates during irradiation process depends on the reaction time of MB solution, which is in good agreement with the results reported in the literature [10, 27-28]. However, the formation rate of aggregates can change related to other experimental conditions such as MB concentration, type of solvent and adsorbent used [29, 30], which are not the purpose of this study. (4) The highest degradation efficiency was obtained by using the coral-like R3-TiO_2 film. Large surface area, 167 m^2/g (see Table 3), associated with high response in the wavelength range of about 450-530 nm (see Fig. 5A), can be seen to be an answer for the high photocatalytic degradation efficiency of coral-like TiO_2 nanostructured films. This result is also confirmed with the SEM images (see Figs. 1 and 2). Therefore, the coral-like TiO_2 nanostructured film provide much more exposed surface region, well facilitating the adsorption and photoreaction of reactants.

Table 4 lists the kinetic parameters and process efficiency for photocatalytic activities of MB dye. The photocatalytic activities of the coral-like TiO_2 nanostructured thin films obtained from samples R 1-5 can be evaluated using the comparison of the rate constants of first order reaction (k_{app1}). According to this table, the following points should be noted: (1) The coral-like R3-TiO_2 nanostructured film reached 95.8% photodegradation performance, while a greater than 64% conversion was observed for the P25-TiO_2 based film after 2 h. (2) The adsorption spectrum of MB follows a pseudo-second-order kinetics model for the first 180 min irradiation. The MB degradation-time curves can be well fitted by a first order kinetics model for 60 min. (3) Above 60 min irradiation, a deviation from the first order kinetics is observed. Therefore, minimum regression coefficients (R^2) of 0.990 and 0.986 are obtained for R2 and R3-TiO_2 films, respectively. (4) Comparison of the rate constants between the different morphologies of coral-like TiO_2 film reveals that, except for the R5-TiO_2 film, other films are improved and vary widely compared with that of P25-TiO_2 based film. In the case of R3-TiO_2 film, the rate constant reaches its maximum value (1.63×10^{-2} min^{-1}) compared to other samples. This is caused by coral-like TiO_2 morphologies with small

particle size formed on the surface of these structures, which leads to a high loading level, narrowing of band gap, and reduced recombination of electron-hole pairs during photocatalysis [31, 32]. This can be attributed to the decrease in volume recombination of charge carriers because of accelerating the interfacial transfer rates. (5) The process efficiency (φ) is defined as the concentration change by amount of energy originating from light intensity and solution irradiated plane surface area. The described efficiency for the degradation of MB using the R3-TiO_2 film showed the highest value of 7.845×10^{-6} ppm/min W cm. The process efficiency of TiO_2 nanostructured films was obtained from different samples irrespective of MB volume usage, corresponding to the order: R3 > R2 > R1 > R4 > R5. (6) The photocatalytic degradation rate constant of MB for the coral-like R3-TiO_2 nanostructured film is 1.63×10^{-2} min^{-1}, which is about 2.5 fold higher than that for the commercial P25-TiO_2 based film, 6.4×10^{-3} min^{-1}, further confirming that the coral-like TiO_2 nanostructured film shows high photocatalytic activity for promising environmental applications.

Photocatalytic degradation of MO.

Fig. 5a illustrates a typical UV-Vis adsorption spectrum of MO azo dye adsorbed on the coral-like R3-TiO_2 nanostructured thin film. The initial concentration of MO solution was adjusted to 5×10^{-5} M. As shown from this figure, the MO shows a maximum absorption at about 471 nm, while the intensity of adsorption peak significantly decreases with the UV irradiation time showing a drop in the orange absorption with reaction time at a wavelength of above ~500 nm, which represents a more adsorption of MO dye on the TiO_2 film surface. Fig. 5b plots the photocatalytic degradation of MO as a function of irradiation time in the presence of coral-like TiO_2 films obtained from samples of R 1-5 (corresponding to curves a-e). For comparison, photocatalytic degradation curve of MB by P25-TiO_2 based film is also studied under the same conditions (curve f). The intensity of the all absorption peaks shows a low degradation rate with irradiation time according to an exponential decay function. This slight degradation rate should be attributed to the presence of UV irradiation. However, the absorption bands show a slight bathochromic shifts by as much as 8 nm from 465 to 473 nm. According to Fig. 5b,

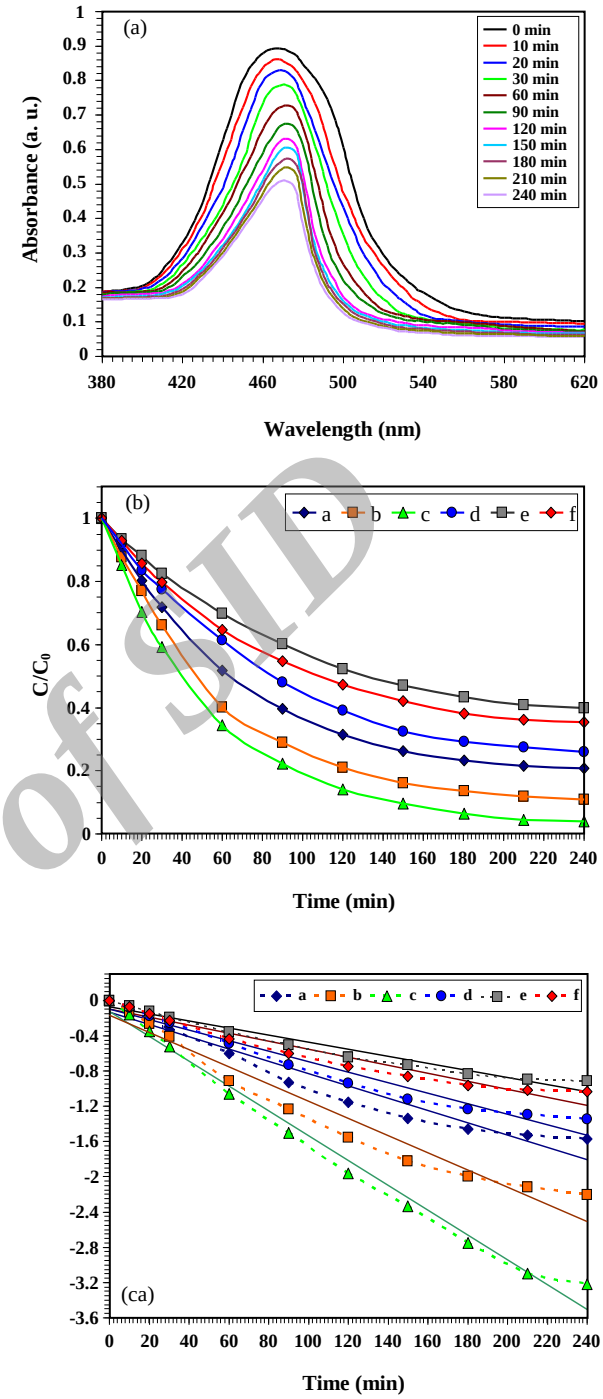

Fig. 5: Photocatalytic activities of coral-like TiO_2 nanostructured thin films in degradation of MO azo dye (5×10^{-5} M). (A) UV-vis spectra of MO adsorbed on the R3-TiO_2 film with different irradiation times as a function of wavelength. (b) Comparison of photocatalytic degradation of MO under UV light irradiation. (c) Pseudo-first-order kinetic rate plots for the photocatalytic degradation of MO. [(a) R1, (b) R2, (c) R3, (d) R4, (e) R5, (f) P25-TiO_2 based film].

Table 4: Kinetic parameters for photocatalytic activities of the coral-like TiO2 nanostructured thin films obtained from different samples (R 1-5) for degradation of MB and MO organic dyes.

Dye type	Kinetic parameters	Samples					
		P25	R1	R2	R3	R4	R5
MB	X_{4h} (%)*	64.6	79.2	89.0	95.8	74.0	60.0
	$K_{app1}\times10^{-3}$, min^{-1}	6.4	10.0	13.4	16.3	7.8	5.4
	R^2	0.994	0.998	0.990	0.986	0.997	0.997
	Rate ratio to P25	1.00±0.00	1.56±0.07	2.10±0.10	2.54±0.11	1.22±0.05	0.85±0.04
	$\varphi\times10^{-6}$ ** (ppm/min W cm)	5.643	6.986	7.564	7.845	6.729	5.514
MO	X_{4h} (%)*	63.4	78.6	86.5	93.4	72.0	59.5
	$K_{app1}\times10^{-3}$, min^{-1}	6.1	9.1	11.1	14.3	7.2	4.8
	R^2	0.997	0.995	0.992	0.989	0.996	0.993
	Rate ratio to P25	1.00±0.00	1.49±0.07	1.82±0.09	2.34±0.10	1.18±0.04	0.79±0.11
	$\varphi\times10^{-6}$ ** (ppm/min W cm)	5.337	6.853	7.175	7.609	6.608	4.762

** Conversion X (%) = [1-(C/C0)]×100.*
*** Process efficiency, φ (ppm/min W cm) = (C0-C/) tIS. (C0-C)*

it can be found that the photocatalytic degradation of MO dye after 240 min UV irradiation was 66.5, 73.7, 82.1, 57.4, and 44.9% for coral-like TiO_2 nanostructured films obtained from samples R1, R2, R3, R4, and R5, respectively. Therefore, the photocatalytic activities of all TiO_2 films, except for R5-TiO_2 film, were higher than that of P25-TiO_2 based film (52.5%).

Fig. 5c shows the determination of rate constant for MO degradation over coral-like TiO_2 thin films obtained from samples of R 1-5 (corresponding to curves a-e) and P25 (curve f). It is suggested that the photo-degradation of MB over the prepared coral-like TiO_2 films at different synthetic conditions follows the pseudo-first-order reaction during 210 min irradiation. According to Fig. 5c, after 210 min irradiation, a deviation (indicated by dashed lines) from the first order kinetics model is observed for all results. The highest deviation was observed for the R3-TiO_2 film (11.23%).

The kinetic parameters and process efficiency for photocatalytic activities of MO dye using different morphologies of coral-like TiO_2 nanostructured thin film are also listed in Table 4. The photocatalytic activities of the TiO_2 thin films obtained from samples R 1-5 are evaluated by comparing their k_1. According to Table 4, the following points should be mentioned: (1) The coral-like R3-TiO_2 nanostructured film reached 93.4% photodegradation performance, while 63.4% conversion was observed for the P25-TiO_2 based film after 2 h. (2) Similar to obtained results for MB dye molecule, the rate constants of all morphologies of coral-like TiO_2 film, except for R5-TiO_2 film, show an improvement in photocatalytic degradation of MO compared with that of P25. (3) The highest rate constant (1.43×10^{-2} min^{-1}) of MO degradation is reported by the R3-TiO_2 film, the reported value of which is about 2.3 fold higher than that for the P25-TiO_2 based film (6.1×10^{-3} min^{-1}). It means that the large surface area of R3-TiO_2 film could provide more active sites and absorb more reactive species. (4) The lowest rate constant (4.8×10^{-3} min^{-1}) of MO degradation is reported for the R5-TiO_2 that is associated with high phase crystallinity (see Fig. 3). The high crystallinity means few defects in the photocatalytic properties of prepared TiO_2 film. It is well known that these defects may act as the recombination sites for photoexcited electron-hole pairs during photocatalysis, which would decrease the photocatalytic activity. (5) All results show a deviation from first order kinetic model as demonstrated by the linear regression analysis. However, minimum R^2 of 0.989 is obtained for the R3-TiO_2 film. (6) The process efficiency (φ) for the degradation of MO using the R3-TiO_2 film showed the highest value of 7.175×10^{-6} ppm/min W cm. However, the process efficiency of TiO_2 nanostructured films obtained from different samples irrespective of MO dye had similar trend to MB (R3 > R2 > R1 > R4 > R5).

The above results clearly show that the coral-like TiO_2 nanostructured film fabricated in this work is an excellent photocatalyst material. Consequently, this work represents a novel method for enhancing photocatalytic degradation of organic dye molecules by thin films. Additionally, by increasing the dimensions of prepared coral-like TiO_2 nanostructured thin film, a larger scale of pollution degradation could be possible. Finally, TiO_2 thin film can be easily withdrawn from the photocatalytic reaction system, while is unachievable with the commercial TiO_2 powder.

CONCLUSIONS

In summary, a facile approach for fabrication of coral-like TiO_2 nanostructured thin films is presented by sol-gel dip-coating technique. The as-synthesized coral-like TiO_2 nanostructures showed a micro, meso and macropore structures with a high specific surface area of 167 m^2/g and mean pore size diameter of 12.3 nm. BET analysis and porosimetry measurements show that the volume of macropores formed on the surface of obtained thin film is considerably larger than the volume of micropore or mesopores. Almost the micro/mesopore structures were mainly obtained from a difference of aggregated voids among the TiO_2 nanoparticles. XRD analysis shows that the dominant crystalline phase of synthesized TiO_2 was anatase (98 wt. %). The Photocatalytic experiment results showed that the thin film obtained from the sample with the TTIP: HF molar ratio of 1:1.5 showed the highest conversion of 95.8 and 93.4 % in MB and MO degradation during UV irradiation, which were 2.5 and 2.3 fold higher than that of the commercial P25-TiO_2 based film, respectively. However, the process efficiency for the degradation of MB and MO dyes using the prepared TiO_2 thin films were determined to be 7.845×10^{-6} and 7.175×10^{-6} ppm/min W cm, respectively. Reduced recombination of electron-hole pairs, small particle size, a pore scattering, reduced band gap energy, high crystallization degree of anatase and short diffusion path for the reactant were responsible for the high photocatalytic activity of the coral-like TiO_2 nanostructured thin film. In addition, coral-like TiO_2 nanostructured thin film can be easily separated from the reaction system, which can avoid separation problems, unlike what happens in the case of the commercial TiO_2 powder. With these features, the coral-like TiO_2 nanostructured thin film exhibits high photocatalytic activity for promising environmental applications such as wastewater treatment and air pollution degradation.

Received : 30 Apr. 2015 ; Accepted : Dec. 7, 2015

REFERENCES

[1] Janitabar Darzi S., Mahjoub A. R., Nilchi A., Synthesis of Spongelike Mesoporous Anatase and Its Photocatalytic Properties, *Iran. J. Chem. Chem. Eng. (IJCCE)*, **29**(2): 37-42 (2010).

[2] Chen Sh.-L., Wang A.-J., Dai Ch., Benziger J. B., Liu X.-Ch. The Effect of Photonic Band Gap on the Photo-catalytic Activity of nc-TiO_2/SnO_2 Photonic Crystal Composite Membranes, *Chem. Eng. J.*, **249**(1): 48-53 (2014).

[3] Wang Sh., Yang J., Zhang H., Wang Y., Gao X., Wang L., Zhu Zh. One-pot Synthesis of 3D Hierarchical SnO_2 Nanostructures and Their Application for Gas Sensor. *Sensor Actuat. B-Chem.*, **207** (Part A): 83-89 (2015).

[4] Mali S. S., Betty Ch. A., Bhosale P. N., Patil P. S., Hong Ch. K. From Nanocorals to Nanorods to Nanoflowers Nanoarchitecture for Efficient Dye-sensitized Solar Cells at Relatively Low Film Thickness: All Hydrothermal Process, *Scientific Reports*, **4** (5329): 1-8 (2014).

[5] Hardin B. E., Hoke E. T., Armstrong P. B., Yum J-H., Comte P., Torres T., Fréchet J. M. J., Nazeeruddin M. Kh., Grätzel M., McGehee M. D. Increased Light Harvesting in Dye-Sensitized Solar Cells with Energy Relay Dyes, *Nat. Photonics*, **3** (1): 406-411 (2009).

[6] Grätzel M. Photoelectrochemical Cells. *Nature*, **414**(1): 338-344 (2001).

[7] Masuda Y., Ohji T., Kato K. Multineedle TiO_2 Nanostructures, Self-assembled Surface Coatings, and Their Novel Properties. *Cryst. Growth & Des.*, **10**(2): 913-922 (2009).

[8] Gnatyuk Y., Smirnova N., Korduban O., Eremenko A., Photoelectrochemical and Photocatalytic Properties of Mesoporous TiO_2 Films Modified with Silver and Gold Nanoparticles, *Surf. Interface Anal.* (*SIA*), **42**(1): 1276-1280 (2010).

[9] Patil S. R., Hameed B. H., Škapin A. S., Štanga U. L. Alternate Coating and Porosity as Dependent Factors for the Photocatalytic Activity of Sol–gel Derived TiO_2 Films. *Chem. Eng. J.*, **174** (1): 190-198 (2011).

[10] Shao X., Lu W., Zhang R., Pan F., Enhanced Photocatalytic Activity of TiO_2-C Hybrid Aerogels for Methylene Blue Degradation. *Sci. Rep*., **3**(1): 1-9 (2013).

[11] Apollo S., Onyongo M. S., Ochieng A. UV/H_2O_2/TiO_2/Zeolite Hybrid System for Treatment of Molasses Wastewater, *Iran. J. Chem. Chem. Eng*. (*IJCCE*), **33**(2): 107-117 (2014).

[12] Rao Y. F., Chu W. Reaction Mechanism of Linuron Degradation in TiO_2 Suspension Under Visible Light Irradiation with the Assistance of H_2O_2. *Environ. Sci. Technol*. (*ES & T*), **43** (16): 6183-6189 (2009).

[13] Chen J., Yang H. B., Miao J., Wang H-Y., Liu B. Thermodynamically Driven One-Dimensional Evolution of Anatase TiO_2 Nanorods: One-Step Hydrothermal Synthesis for Emerging Intrinsic Superiority of Dimensionality. *J. Am. Chem. Soc*. (*JACS*), **136**(43): 15310-15318 (2014).

[14] Yu J., Yu J. C., Leung M. K. P., Ho W., Cheng B., Zhao X., Zhao J. Effects of Acidic and Basic Hydrolysis Catalysts on the Photocatalytic Activity and Microstructures of Bimodal Mesoporous Titania. *J. Catal*., **217** (1): 69-78 (2003).

[15] Liu M., Piao L., Wang W. Fabrication and Characteristics of Three-Dimensional Flower-like Titanate Nanostructures, *J. Nanosci. Nanotechnol*. (*JNN*), **10** (11): 7469-7472 (2010).

[16] Zheng Z. K., Huang B. B., Qin X. Y., Zhang X. Y., Dai Y. Strategic Synthesis of Hierarchical TiO_2 Microspheres with Enhanced Photocatalytic Activity, *Chem. Eur. J*., **16** (37): 11266-11270 (2010).

[17] Duong T., Phan N., Kim E. J., Hahn S. H., Kim W. J., Shin E. W. J. Synthesis of Hierarchical Rose Bridal Bouquet- and Humming-top-like TiO_2 Nanostructures and Their shape-dependent Degradation Efficiency of Dye. *Colloid Interface Sci*. (*COCIS*), **356** (1): 138-144 (2011).

[18] Tian G. H., Chen Y. J., Zhou W., Pan K. Tian C. G., Huang X. R., Fu H. G. 3D Hierarchical Flower-like TiO_2 Nanostructure: Morphology Control and Its Photocatalytic Property. *Cryst. Eng Comm.*, **13** (1): 2994-3000 (2011).

[19] Bahramian A. High Conversion Efficiency of Dye-sensitized Solar Cells Based on Coral-like TiO_2 Nanostructured Films: Synthesis and Physical Characterization. *Ind. Eng. Chem. Res*. (*I&EC*), **52**(42): 14837-14846 (2013).

[20] Wong E.M., Bonevich, J.E., Searson P.C., Growth Kinetics of Nanocrystalline ZnO Particles from Colloidal Suspensions, *J. Phys. Chem. B*, (*JPCB*), **102** (40): 7770-7775 (1998).

[21] Liu B., Zeng H.C., Fabrication of ZnO "Dandelions" Via a Modified Kirkendall Process, *J. Am. Chem. Soc*. (*JACS*), **126** (51): 16744-16746 (2004).

[22] Liyong W., Yuanyuan H., Shiwen D., Photo-Catalytic Nanometer Composite-Crystal TiO_2 Powder Synthesized by Two-Step Method, *Iran. J. Chem. Chem. Eng*. (*IJCCE*), **29** (3): 13-17 (2010).

[23] Kolenko Y. V., Burukhin A. A., Churagulov B. R., Oleynikov N. N. Synthesis of Nanocrystalline TiO_2 Powders from Aqueous $TiOSO_4$ Solutions Under Hydrothermal Conditions. *Mater. Lett*., **57**(5-6): 1124-1129 (2003).

[24] An R., Yu Q., Zhang L., Zhu Y., Guo X., Fu S., Li L., Wang C., Wu X., Liu C., Lu X. Simple Physical Approach to Reducing Frictional and Adhesive Forces on a TiO_2 Surface via Creating Heterogeneous Nanopores. *Langmuir*, **28** (43): 15270-15277 (2012).

[25] Gregg S. J., Sing, K. S. W. "Adsorption, Surface Area and Porosity", Academic Press, London, (1982).

[26] Kumar K.V., Porkodi K., Rochaa F., Langmuir-Hinshelwood Kinetics- A theoretical Study. *Catalysis Commun*, **9** (1): 82-84 (2008).

[27] Yang G., Hu P., Cao Y., Yuan F., Xu R. Fabrication of Porous TiO(2) Hollow Spheres and Their Application in Gas Sensing. *Nanoscale Res Lett*., **5**(9): 1437-1441 (2010).

[28] K. Murugan, T. N. Rao, A. S. Gandhi, B. S. Murty. Effect of Aggregation of Methylene Blue Dye on TiO_2 Surface in Self-Cleaning Studies, *Catalysis Commun*., **11** (6): 518-521 (2010).

[29] Wu Ch-H., Chern J-M. Kinetics of Photocatalytic Decomposition of Methylene Blue. *Ind. Eng. Chem. Res*. (*I&EC*), **45** (19): 6450-6457 (2006).

[30] Samarghandi M.R., Zarrabi M., Noori Sepehr M., Panahi R., Foroghi M. Removal of Acid Red 14 by Pumice Stone as A Low Cost Adsorbent: Kinetic and Equilibrium Study, *Iran. J. Chem. Chem. Eng*. (*IJCCE*), 31 (3): 19-27 (2012).

[31] Robles-Águila M.J., Elizalde-González M.P., Mendoza M.E., Silva-González R., Yee-Madeira H., Bulk and Surface Analysis of $Ti_{1-x}Fe_xO_2/Fe_2O_3$ Composites Prepared by Solid State Reaction for Photocatalytic Applications, *Surf. Interface Anal.* (*SIA*), **44** (1): 484-490 (2012).

[32] Simin Janitabar Darzi; Maryam Movahedi, Visible Light Photodegradation of Phenol Using Nanoscale TiO_2 and ZnO Impregnated with Merbromin Dye: A Mechanistic Investigation, *Iran. J. Chem. Chem. Eng.* (*IJCCE*), **31** (2): 55-64 (2014).